Hindawi Publishing Corporation
Mathematical Problems in Engineering
Volume 2015, Article ID 204730, 13 pages
http://dx.doi.org/10.1155/2015/204730

*Research Article*

# Numerical Limit Load Analysis of 3D Pressure Vessel with Volume Defect Considering Creep Damage Behavior

**Xianhe Du,[1] Donghuan Liu,[2] and Yinghua Liu[1]**

[1]*School of Aerospace Engineering, AML, Tsinghua University, Beijing 100084, China*
[2]*Department of Applied Mechanics, University of Science and Technology Beijing, Beijing 100083, China*

Correspondence should be addressed to Yinghua Liu; yhliu@tsinghua.edu.cn

Received 14 September 2014; Accepted 27 November 2014

Academic Editor: Chenfeng Li



The limit load of 3D 2.25Cr-1Mo steel pressure vessel structures with volume defect at 873 K is numerically investigated in the present paper, and limit load under high temperature is defined as the load-carrying capacity after the structure serviced for a certain time. The Norton creep behavior with Kachanov-Robotnov damage law is implemented in ABAQUS with CREEP subroutine and USDFLD subroutine. Effect of dwell time to the material degradation of 2.25Cr-1Mo steel has been considered in this paper. 190 examples for the different sizes of volume defects of pressure vessels have been calculated. Numerical results showed the feasibility of the present numerical approach. It is found that the failure mode of the pressure vessel depends on the size of the volume defect and the service life of the pressure vessel structure at high temperature depends on the defect ratio seriously.

## 1. Introduction

With the rapid development of modern industry, the world demand for power supplies will increase by up to 50% in the next 20 years [1]. Thus, developing effective energy resources becomes essential. The effective energy sources always come from nuclear power plants, fossil fired power plants, and petrochemical industries. In these fields, pressure vessel and piping structures are always used at high temperature for a long time. Meanwhile, it cannot be avoided that the high temperature devices contain volume defects result from welding, polishing, corrosion, and oxidation in the manufacture, assembling, and operation procedures. The volume defects include slag inclusion, volume pit, and pore, which can reduce the strength of structures and even lead to the leaking and explosion accident. The limit analysis for the structure with volume defect is very important in structure safety assessment. Through limit analyzing, the limit load of structure can be obtained which is a theoretical foundation for rational design and safety assessment of pressure vessel and piping. The limit analysis of structure is also an important and practical branch of plastic mechanics, whose theory foundation was established at the beginning of 1910s. In 1950s, the complete theory of upper and lower bound for limit analysis was presented by Drucker and Hill [2, 3]. In this theory, perfect plastic, small deformation, and proportional loading were assumed for simplifying the limit analysis. Hodge and Belytschko [4–6] studied the plastic limit analysis for plane and axial symmetry shell structures. Maier and Munro [7] reviewed the engineering application of plastic limit analysis. However, these researches were just based on beam, symmetry structure, and plane problem. For the complex structures in engineering, it is difficult to obtain the analytical solution because of the discontinuity of geometry and complex loading; therefore, the limit analysis was hard to complete.

With the development of computer hardware and finite element method, the limit analysis for complex structure can be carried out using numerical method. In 1965, Koopman and Lance [8] studied the plastic limit load using nonlinear mathematical programming firstly. Then, Lance and Koopman [9] used this method to analyze the 2D plate and symmetry shell structure. Maier et al. [10] used the method of successive linear approximation to the yield surface, which converted the nonlinear mathematical programming to multiple linear mathematical programming. In 1981,

Christiansen [11, 12] presented a mathematical programming method to complete the limit analysis using hybrid finite element to approach infinite dimension based on von Mises yield criterion. Berak and Gerdeen [13] presented a P-norm method based on lower bound method of limit load, and then Chen [14] developed the P-norm method and proposed a dimension reduced iteration method to complete the limit analysis for pressure vessel structure with volume defect. Mackenzie et al. [15] proposed a simple method, named the elastic compensation method, to estimate the limit load of pressure vessel structure. In this method, upper and lower bound method was not used; nevertheless, a series of elastic direct iterations were applied to obtain the limit load, which is convenience for engineering application. Liu et al. [16–25] used the penalty-duality algorithm and direct iteration method to analyze the limit load of 3D structure. The pressure vessels with volume defects were analyzed, and the failure modes for different defects were presented. A series of numerical results and fitting curves of limit load were given, which indicated the numerical method for limit analysis of complex structures was available, feasible, and reasonable. However, the researches of limit load were done at room temperature condition. With the pressure vessels being widely used in high temperature fields, the limit analysis for these structures with volume defects would become more significant.

In the high temperature environment, ferritic steels, such as Cr-Mo steel, are used extensively as structural materials of pressure vessel. Pressure vessel components operating at high temperatures are subjected to creep damage, which results from the formation, growth, and coalescence of cavities and also from the enhanced microstructural degradation in the form coarsening of precipitates and dislocation substructure under stress [26]. Recently, several studies have been performed to investigate and model the creep damage behavior in Cr-Mo steel. Al-Faddagh et al. studied the effect of state of stress on creep behavior of 2.25Cr-1Mo steel [27]. Wu et al. [28] carried out the numerical analysis to study the influence of constraint on creep behavior in notched bars considering various factors. Ray et al. [29] reported the long term creep-rupture behavior of 2.25Cr-1Mo steel between 773 and 873 K. Basirat et al. [1] carried out a study of the creep behavior of modified 9Cr-1Mo steel using continuum-damage modeling. Goyal et al. studied the creep cavitation and rupture behavior of 2.25Cr-1Mo steel [30]. Results showed that the creep damage would increase with the increment of stress level, and the tensile strength and yield stress would decrease with the increment of temperature and creep damage. It is worth noting that the yield stress reduction would lead to the limit load reduction, which means the limit load calculation of pressure vessel structure at high temperature would depend on temperature, creep damage, and different stress levels. However, few researchers had considered the aspects above in the limit analysis of pressure vessel structure at high temperature.

In the present paper, limit load under high temperature is defined as the load-carrying capacity after the structure serviced for a certain time, and limit analysis of pressure vessel structure at 873 K has been numerically studied. The material is 2.25Cr-1Mo steel and Norton creep behavior with Kachanov-Robotnov damage law has been implemented in ABAQUS by the CREEP subroutine and USDFLD subroutine, and yield stress reduction due to temperature, creep damage, and different stress levels is also considered here. Meanwhile, effects of volume defects sizes to the limit load are given.

## 2. Finite Element Model

*2.1. Creep Constitutive Model with Continuum Damage Mechanics Law.* At high temperature, creep deformation was dominated and the redistribution of stresses was found to be dependent on the creep constitutive laws obeyed by the material [30]. Typical creep deformation includes three regimes, primary, secondary, and tertiary creep regimes. For the purpose of easy application, Yatomi et al. [31–34] and Oh et al. [35] proposed a model which is similar to Norton's law and considers the average creep strain rate, $\dot{\varepsilon}^c$, in their researches. The simplest model has been written in the power-law form as

$$\dot{\varepsilon}^c = A\sigma^n, \tag{1}$$

where $A$ and $n$ are the creep coefficient and exponent of material constants, respectively. $\sigma$ denotes the equivalent (von Mises) stress. In order to describe the entire creep curves accurately, Oh et al. [36] used a strain-hardening creep law composed of three terms

$$\dot{\varepsilon}^c = A_1\sigma^{n_1}\varepsilon_c^{m_1} + A_2\sigma^{n_2}\varepsilon_c^{m_2} + A_3\sigma^{n_3}\varepsilon_c^{m_3}, \tag{2}$$

where $A_1$, $A_2$, $A_3$, $n_1$, $n_2$, $n_3$, $m_1$, $m_2$, and $m_3$ are the material constants from creep experiment data and $\varepsilon_c$ denotes the equivalent creep strain. Although the creep curves dependent on these phenomenological creep laws agree with the creep data well when creep softening is a consequence of plastic strain, it cannot be proper for materials subjects to damage mechanisms [37]. However, the continuum damage mechanics (CDM) constitutive may be more reasonable because it takes account of degradation mechanisms.

Kachanov [38] and Rabotnov [39] model has been widely accepted and used for predicting the tertiary creep behavior of the material, and the creep strain rate is defined by the following equation:

$$\dot{\varepsilon}_{ij}^c = \frac{3}{2}A\left(\frac{\sigma}{1-\omega}\right)^n \frac{s_{ij}}{\sigma}, \tag{3}$$

where $A$ and $n$ are material constants in Norton's law, $\dot{\varepsilon}_{ij}^c$ and $s_{ij}$ are the creep strain rate tensor and deviatoric stress tensor, respectively, and $\omega$ is the damage parameter varying from 0 to 1 indicating virgin material and fully damaged material, respectively.

The creep damage evolution equation as a function of stress and current damage is described by the following equation:

$$\dot{\omega} = \frac{B\sigma_r^\chi}{(1-\omega)^\phi}, \tag{4}$$

Table 1: Chemical composition for 2.25Cr-1Mo steel at 873 K (wt%) [30].

| Material | C | Si | Mn | P | S | Cr | Mo | Fe |
|---|---|---|---|---|---|---|---|---|
| 2.25Cr-1Mo steel | 0.06 | 0.18 | 0.48 | 0.008 | 0.008 | 2.18 | 0.93 | Bal |

Table 2: Creep and damage constants for 2.25Cr-1Mo steel at 873 K [30].

| $E$ (MPa) | $\nu$ | $A$ | $n$ | $\chi$ | $\phi$ | $B$ | $\alpha$ |
|---|---|---|---|---|---|---|---|
| 160000 | 0.3 | $9.17 \times 10^{-17}$ | 6.02 | 6.69 | 4.8 | $0.91 \times 10^{-17}$ | 0.01 |

where $B$, $\chi$, and $\phi$ are material constants, and $\sigma_r$ is the rupture stress defined by [40]

$$\sigma_r = \alpha\sigma_1 + (1-\alpha)\,\sigma, \tag{5}$$

where $\sigma_1$ is maximum principle stress, $\alpha$ is a material constant which describes the effect of multiaxial stress states, and $\sigma$ denotes the equivalent stress. It was found that high stress level would lead to high creep strain rate and creep damage; in the present paper, high stresses are mainly caused by volume defects and the effects of different shape parameter of volume defect are considered.

Finite element analysis of creep deformation was carried out using the commercial codes ABAQUS [41]. To define the time-dependent and creep damage behavior, (3)–(5) have been implemented into the ABAQUS user subroutine CREEP. The rupture stress was calculated from von-Mises stress and maximum principle stress. The von-Mises stress can be obtained from CREEP subroutine. However, in order to get the maximum principle stress, USDFLD and GETVRM subroutines were used. The detail simulation technique about how the three subroutines worked collaboratively is illustrated in Section 2.3. Compositions of chemical component and material properties for 2.25Cr-1Mo steel at 873 K are listed in Tables 1 and 2, respectively. It should be pointed out that the Kachanov-Robotnov model coding by CREEP subroutine has been earlier successfully to evaluate the damage evolution under creep condition [42].

*2.2. Elastic-Plastic Material Properties.* The calculation of limit load is dependent on the yield stress of material. However, the yield stress of 2.25Cr-1Mo steel material is not a constant at high temperature under creep condition. It is revealed that the tensile strength and yield stress would decrease with the temperature and creep damage increase [43]. The yield stress reduction would lead to the limit load reduction, which means the limit load calculation of pressure vessel structure at high temperature would be dependent on temperature and creep damage.

The elastic perfectly-plastic model is used for calculating limit load in current work. The reduced yield stresses (RYS) for 2.25Cr-1Mo at 873 K are obtained from ASME codes NH-III which fits for class 1 components in elevated temperature service [43], and fitting function of the yield stress curve when creep dwell time is larger than 300 hours is described by the following equation:

$$\sigma_s^t = [-0.075\ln(t) + 1.4164]\,\sigma_{s0}, \tag{6}$$

where $\sigma_{s0}$, $t$, and $\sigma_s^t$ are initial yield stress, dwell time, and time-dependent reduced yield stress for 2.25Cr-1Mo steel at 873 K, respectively. Considering the creep damage would also cause the reduction of yield stress, the time-dependent and creep damage-coupled yield stress is described below

$$\sigma_s^{te} = (1-\omega)\,\sigma_s^t, \tag{7}$$

where $\sigma_s^{te}$ denotes the effective yield stress considered temperature and creep damage. The plastic material properties for 2.25Cr-1Mo steel at 873 K are listed in Table 3.

To define the time-dependent plastic behavior, the USDFLD subroutine was used to obtain the dwell time and step time at each time increment beginning and then redefine the yield stress by changing Field 1 value. The effective yield stress coupled with creep damage was controlled by Field 2 value. The detailed simulation technique steps for limit load calculation coupled with temperature and creep damage in present work are described in the next section.

*2.3. Simulation Technique Steps.* There are totally three simulation technique steps for limit analysis in this paper, which is described in detail as below and overall structure of the limit analysis solution is shown in Figure 1. Figure 2 shows the load history of the three steps.

*Step 1* (start-up period). Normal working loads, such as internal pressure and axial force, were applied on the cylindrical shell pressure vessel structure with different shape of volume defect, and USDFLD subroutine was called to define the Young's module $E$, Possion ratio $\nu$, and yield stress $\sigma_{s0}$ of virgin material of 2.25Cr-1Mo steel.

*Step 2* (normal service period). In this step, results from Step 1 would be used to define the initial state for the coupled creep damage and time-dependent plastic calculation. USDFLD subroutine was used to obtain the dwell time and step time at each time increment beginning and then redefine the yield stress by setting Field 1 value based on Table 3. Meanwhile, GETVRM subroutine was called in USDFLD to obtain maximum principle stress and pass it into CREEP subroutine for calculating the rupture stress by (5) at each time increment. When the rupture stress and von-Mises stress were obtained, damage accumulation was determined by (4), and the creep strain rate was calculated by (3). The creep strain rate and damage were updated at each end of increment and passed on to ABAQUS, if the damage is larger than 1.0, and the calculation would stop.

*Step 3* (limit analysis period). In this step, stress field at the end of Step 2 was defined as initial state for limit analysis. USDFLD subroutine was used again to get creep damage parameter for calculating the effective yield stress by (7). The yield stress was replaced by effective yield stress by setting Field 2 value similar as Field 1 for limit analysis. When Step 3

Table 3: Plastic material properties for 2.25Cr-1Mo steel at 873 K [43].

| Dwell time (hours) | 0 | 100 | 300 | 1000 | 3000 | 10000 | 30000 | 100000 |
|---|---|---|---|---|---|---|---|---|
| Yield stress (MPa) | 139.00 | 139.00 | 137.61 | 125.10 | 119.97 | 113.41 | 100.86 | 89.41 |
| Field 1 | 0 | 0 | 1 | 2 | 3 | 4 | 5 | 6 |

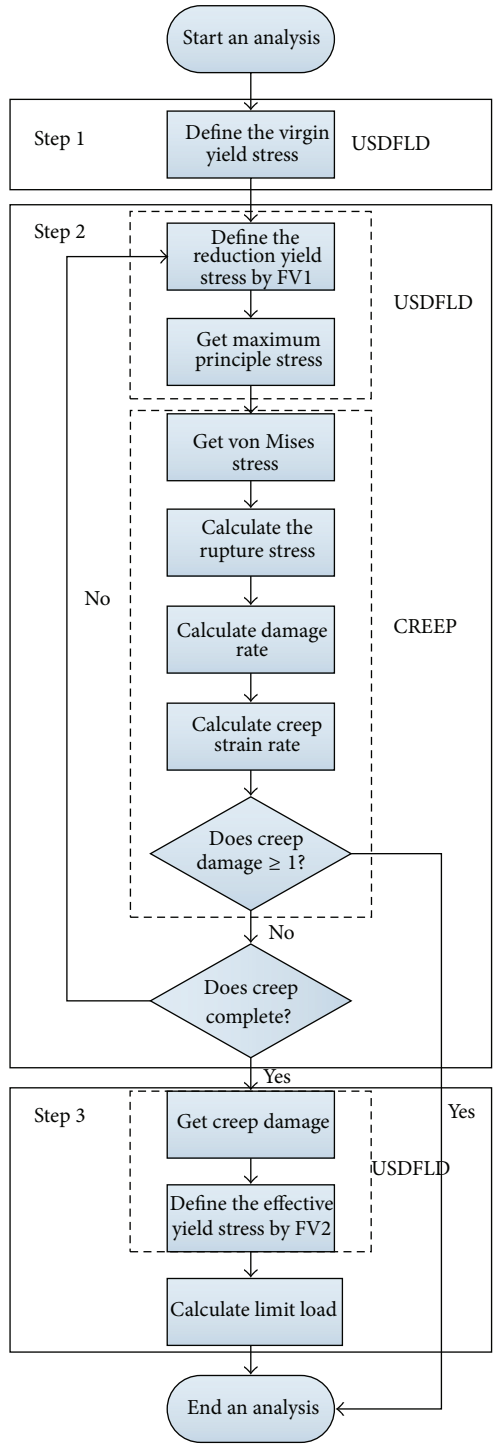


Figure 1: Overall structure of the limit analysis solution.

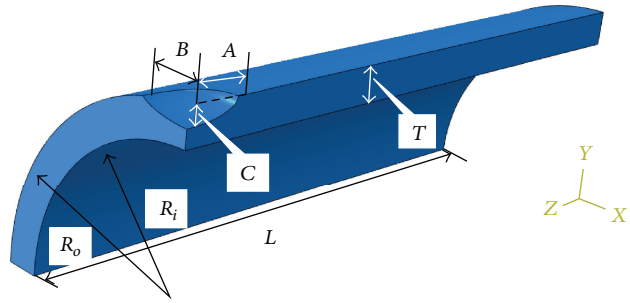


Figure 2: Dimensions of the cylindrical shell pressure vessel with volume defect.

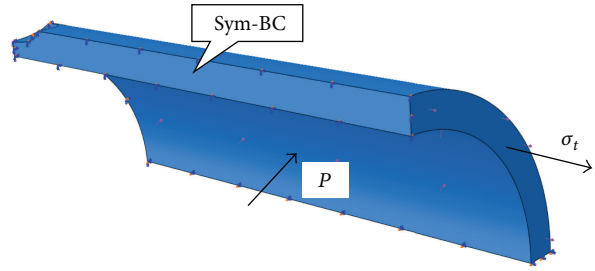


Figure 3: Boundary condition and applied loading of the pressure vessel structure.

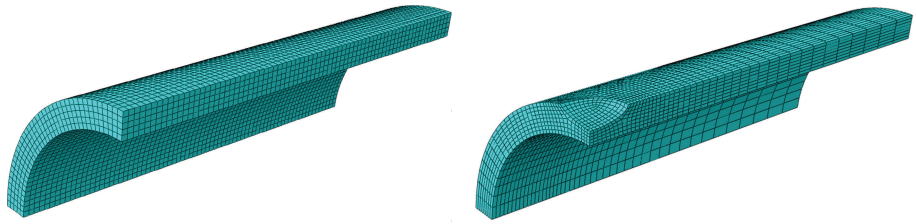

Figure 4: The FE mesh for 3D symmetric model.

was completed, the limit analysis of pressure vessel structure at high temperature had been done.

*2.4. Geometry of the Cylindrical Shell Pressure Vessel with Volume Defect.* Because of the symmetry of the structure, one quadrant of the pressure vessel has been modeled. The geometry of the cylindrical shell pressure vessel with volume defect is shown schematically in Figure 2, where $R_o$ is the outer radius of the cylindrical shell, $R_i$ is the inner radius of the cylindrical shell, $T$ is the wall thickness of the cylindrical shell, $L$ is the length of cylindrical shell, $A$ and $B$ are the half of axial and circumferential length of the volume defect, respectively, and $C$ is the depth of the volume defect.

Define, respectively, the dimensionless axial length of the volume defect as $a = A/B$, the dimensionless circumferential length of the volume defect as $b = C/B$, the dimensionless depth of the volume defect as $c = C/T$, and the ratio of outer radius versus inner radius of cylindrical shell as $K = R_o/R_i$. The basic geometry parameters are listed in Table 4. In order to calculate the limit load of cylindrical shell pressure vessel structure with different shape parameter of volume defect and dwell time, the following nondimension parameters were considered:

Table 4: The basic geometry parameters of cylindrical shell pressure vessel structure.

| $R_o$ (mm) | $R_i$ (mm) | $L$ (mm) | $T$ (mm) | $K$ |
|---|---|---|---|---|
| 550 | 460 | 1500 | 90 | 1.20 |

$a$, dimensionless axial length of the volume defect, whose values are 1.0, 3.0, and 5.0,

$b$, dimensionless circumferential length of the volume defect, whose values are 1/1, 1/3, and 1/4,

$c$, dimensionless depth of the volume defect, whose values are 0.33, 0.5, and 0.6,

$t$, dwell time (hours), whose values are 0, 100, 300, 1000, 3000, 10000, and 30000.

*2.5. Boundary Condition and Applied Loading.* The symmetric boundary conditions (Sym-BC) have been applied on the symmetry surface. The boundary condition and applied loading of the cylindrical shell pressure vessel structure are

Table 5: The numerical limit load results of cylindrical shell pressure vessel structure.

| Number | $A$ (mm) | $B$ (mm) | $C$ (mm) | $a$ | $b$ | $c$ | Dwell time $t$ (hour) Limit load ratio $\overline{P_L}$ 0 | 100 | 300 | 1000 | 3000 | 10000 | 30000 | Rupture time $t_r$ (hour) |
|---|---|---|---|---|---|---|---|---|---|---|---|---|---|---|
| 1 | 29.7 | 29.7 | 29.7 | 1.0 | 1/1 | 0.33 | 0.991 | 0.991 | 0.981 | 0.891 | 0.851 | 0.791 | 0.649 | — |
| 2 | 45 | 45 | 45 | 1.0 | 1/1 | 0.5 | 0.979 | 0.979 | 0.969 | 0.880 | 0.841 | 0.782 | 0.628 | — |
| 3 | 54 | 54 | 54 | 1.0 | 1/1 | 0.6 | 0.969 | 0.969 | 0.959 | 0.871 | 0.832 | 0.773 | 0.597 | — |
| 4 | 89.1 | 89.1 | 29.7 | 1.0 | 1/3 | 0.33 | 0.972 | 0.972 | 0.962 | 0.874 | 0.835 | 0.777 | 0.614 | — |
| 5 | 135 | 135 | 45 | 1.0 | 1/3 | 0.5 | 0.918 | 0.918 | 0.909 | 0.827 | 0.790 | 0.724 | — | 23363.1 |
| 6 | 162 | 162 | 54 | 1.0 | 1/3 | 0.6 | 0.875 | 0.874 | 0.865 | 0.787 | 0.750 | 0.657 | — | 16601.3 |
| 7 | 118.8 | 118.8 | 29.7 | 1.0 | 1/4 | 0.33 | 0.959 | 0.959 | 0.949 | 0.863 | 0.824 | 0.766 | 0.566 | — |
| 8 | 180 | 180 | 45 | 1.0 | 1/4 | 0.5 | 0.882 | 0.882 | 0.873 | 0.794 | 0.757 | 0.673 | — | 17641.9 |
| 9 | 216 | 216 | 54 | 1.0 | 1/4 | 0.6 | 0.808 | 0.808 | 0.800 | 0.726 | 0.682 | — | — | 9288.19 |
| 10 | 89.1 | 29.7 | 29.7 | 3.0 | 1/1 | 0.33 | 0.977 | 0.976 | 0.966 | 0.878 | 0.839 | 0.781 | 0.631 | — |
| 11 | 135 | 45 | 45 | 3.0 | 1/1 | 0.5 | 0.934 | 0.934 | 0.925 | 0.841 | 0.804 | 0.743 | — | 29062.8 |
| 12 | 162 | 54 | 54 | 3.0 | 1/1 | 0.6 | 0.895 | 0.894 | 0.886 | 0.806 | 0.769 | 0.693 | — | 20194 |
| 13 | 267.3 | 89.1 | 29.7 | 3.0 | 1/3 | 0.33 | 0.906 | 0.906 | 0.897 | 0.816 | 0.780 | 0.710 | — | 21210.5 |
| 14 | 405 | 135 | 45 | 3.0 | 1/3 | 0.5 | 0.770 | 0.770 | 0.762 | 0.693 | 0.637 | — | — | 6067.32 |
| 15 | 489 | 163 | 54 | 3.0 | 1/3 | 0.6 | 0.665 | 0.664 | 0.656 | 0.576 | — | — | — | 2111.44 |
| 16 | 356.4 | 118.8 | 29.7 | 3.0 | 1/4 | 0.33 | 0.875 | 0.875 | 0.867 | 0.788 | 0.754 | 0.669 | — | 17402 |
| 17 | 540 | 180 | 45 | 3.0 | 1/4 | 0.5 | 0.708 | 0.708 | 0.701 | 0.630 | 0.531 | — | — | 3725.64 |
| 18 | 648 | 216 | 54 | 3.0 | 1/4 | 0.6 | 0.592 | 0.592 | 0.576 | — | — | — | — | 857.358 |
| 19 | 148.5 | 29.7 | 29.7 | 5.0 | 1/1 | 0.33 | 0.960 | 0.960 | 0.951 | 0.864 | 0.826 | 0.768 | 0.598 | — |
| 20 | 225 | 45 | 45 | 5.0 | 1/1 | 0.5 | 0.885 | 0.885 | 0.876 | 0.797 | 0.761 | 0.682 | — | 19267.5 |
| 21 | 270 | 54 | 54 | 5.0 | 1/1 | 0.6 | 0.816 | 0.816 | 0.808 | 0.734 | 0.690 | — | — | 7484.9 |
| 22 | 445.5 | 89.1 | 29.7 | 5.0 | 1/3 | 0.33 | 0.865 | 0.865 | 0.857 | 0.780 | 0.746 | 0.660 | — | 17256.3 |
| 23 | 675 | 135 | 45 | 5.0 | 1/3 | 0.5 | 0.692 | 0.692 | 0.685 | 0.615 | 0.498 | — | — | 3410.49 |
| 24 | 810 | 162 | 54 | 5.0 | 1/3 | 0.6 | 0.586 | 0.586 | 0.571 | — | — | — | — | 999.066 |
| 25 | 594 | 118.8 | 29.7 | 5.0 | 1/4 | 0.33 | 0.821 | 0.821 | 0.813 | 0.740 | 0.705 | 0.573 | — | 12335 |
| 26 | 900 | 180 | 45 | 5.0 | 1/4 | 0.5 | 0.646 | 0.645 | 0.638 | 0.563 | — | — | — | 2324.28 |
| 27 | 1080 | 216 | 54 | 5.0 | 1/4 | 0.6 | 0.524 | 0.523 | 0.489 | — | — | — | — | 512.07 |

shown in Figure 3, where $P$ is the internal pressure which is 9.8 MPa and $\sigma_t$ denotes the axial force as given below

$$\sigma_t = \frac{PR_i^2}{R_o^2 - R_i^2} = \frac{9.8 \times 460^2}{550^2 - 460^2} = 22.81 \text{ MPa}. \quad (8)$$

*2.6. Mesh and Limit Load Validation.* The FE mesh for 3D symmetric model of the pressure vessels is shown in Figure 4. Since the shape of volume defect is different with each FE model, element numbers of pressure vessels are ranging from 10000 to 15000, about 5 to 8 elements are meshed along the thickness direction to simulate the stress level gradient in this direction, and the element type is C3D20R.

The analytical solution of limit load $P_{L0}$ for the cylindrical shell pressure vessel under room temperature with no defect is given as

$$P_{L0} = \frac{2}{\sqrt{3}}\sigma_s \ln\left(\frac{R_i}{R_0}\right) = \frac{2}{\sqrt{3}} \times 139 \times \ln\left(\frac{550}{460}\right) = 28.68 \text{ MPa}. \quad (9)$$

The numerical solution of limit load is $P_L = 28.53$ MPa, and the relative error is 0.51%. The relative error is less than 1% which indicates the reliability of the numerical solution of limit load using ABAQUS.

## 3. Results and Discussion

*3.1. Nondimensionalization of Results.* In order to avoid the influence of different yield stress and reduce the number of variables, the limit load ratio is defined as

$$\overline{P_L} = \frac{P_L}{P_{L0}}, \quad (10)$$

where $\overline{P_L}$, $P_L$, and $P_{L0}$ are the limit load ratio, current limit load, and limit load of perfect structure. The other nondimensional parameters have been defined in Section 2. The numerical analyses for limit loads of cylindrical shell pressure vessel structure with volume defect have been done using the finite element software ABAQUS. In order to analyze the effects of different stress levels caused by volume

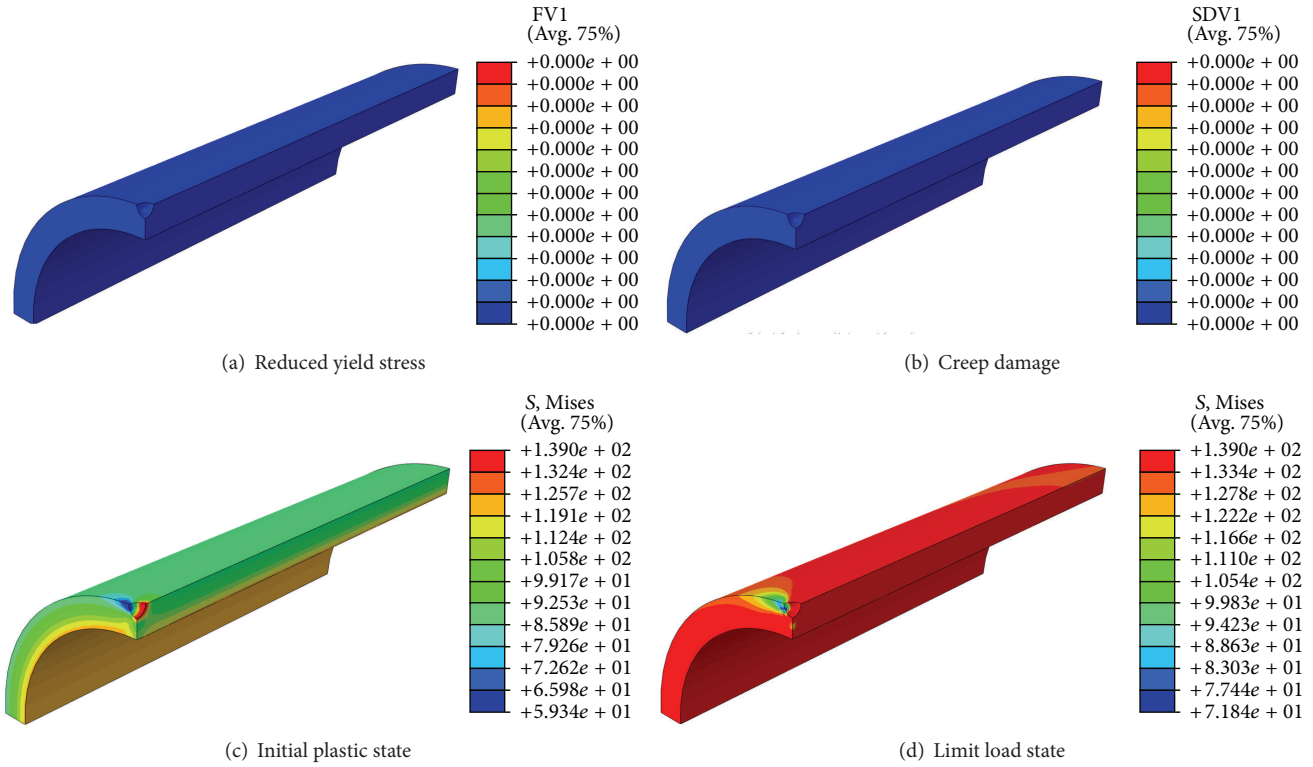


(a) Reduced yield stress (b) Creep damage

(c) Initial plastic state (d) Limit load state

Figure 5: The extension of plastic zone of cylinder shell with volume defect outside ($K = 1.20$, $a = 1.0$, $b = 1/1$, $c = 0.33$, and $t = 0$).

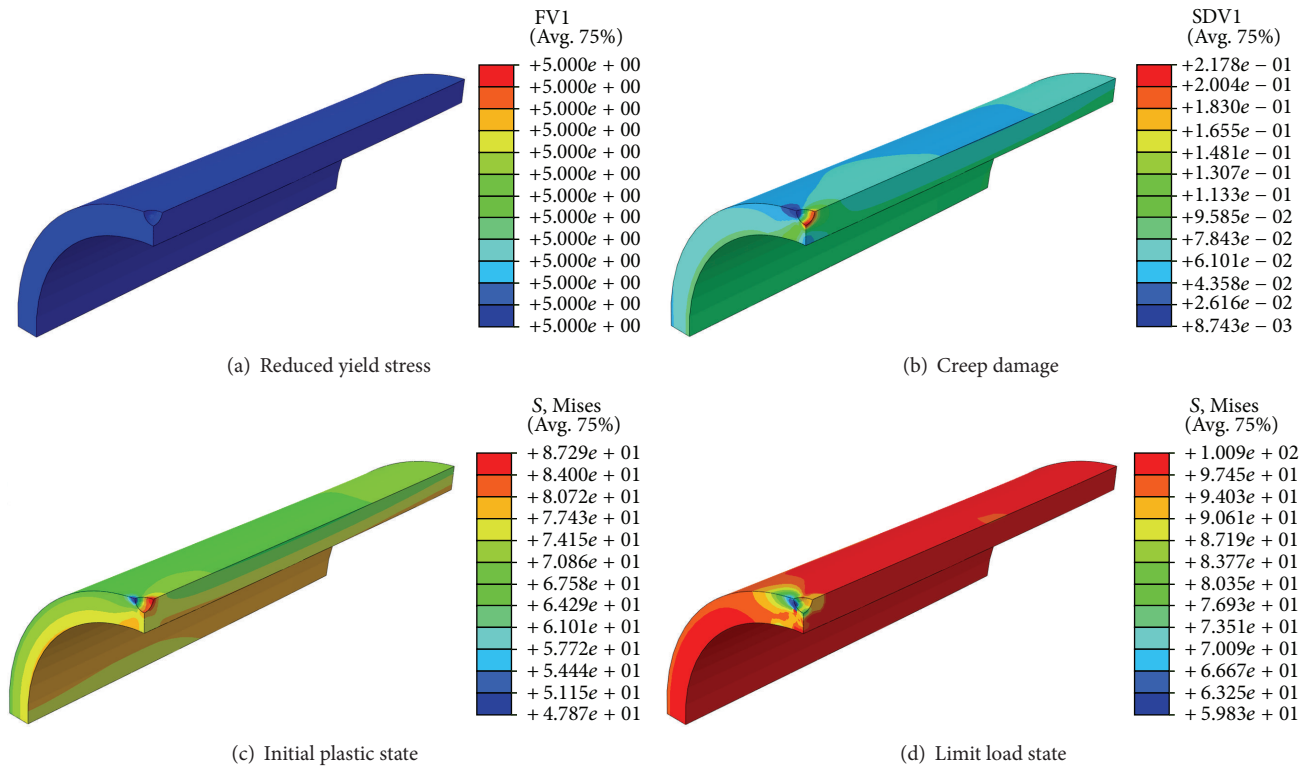


(a) Reduced yield stress (b) Creep damage

(c) Initial plastic state (d) Limit load state

Figure 6: The extension of plastic zone of cylinder shell with volume defect outside ($K = 1.20$, $a = 1.0$, $b = 1/1$, $c = 0.33$, and $t = 30000$ h).

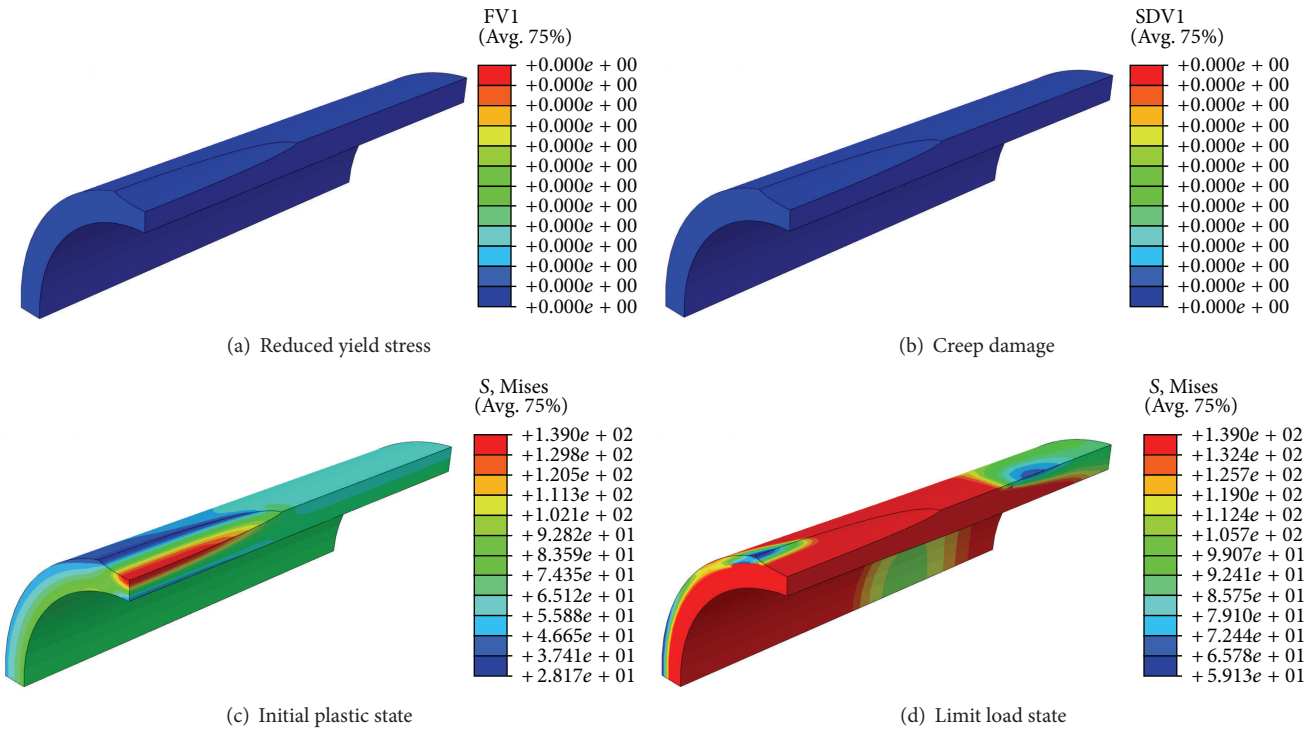


Figure 7: The extension of plastic zone of cylinder shell with volume defect outside ($K = 1.20$, $a = 5.0$, $b = 1/4$, $c = 0.33$, and $t = 0$).

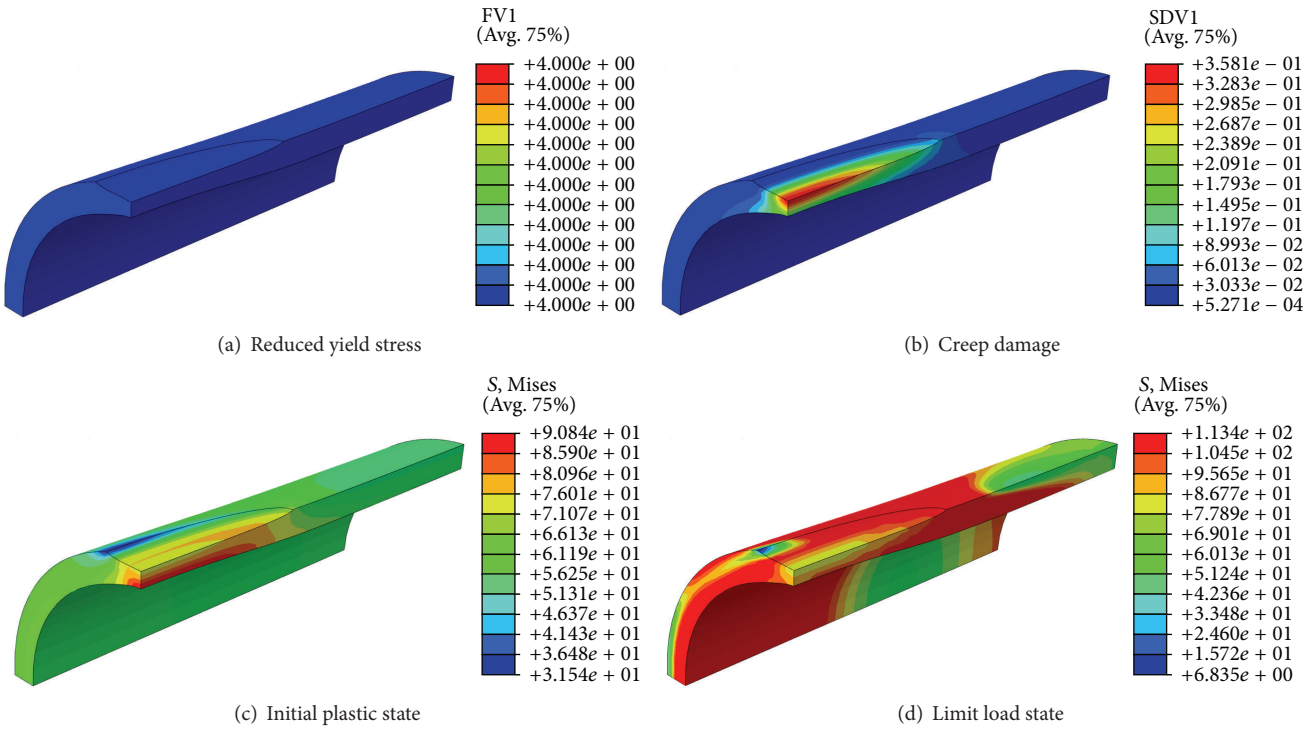


Figure 8: The extension of plastic zone of cylinder shell with volume defect outside ($K = 1.20$, $a = 5.0$, $b = 1/4$, $c = 0.33$, and $t = 10000$).

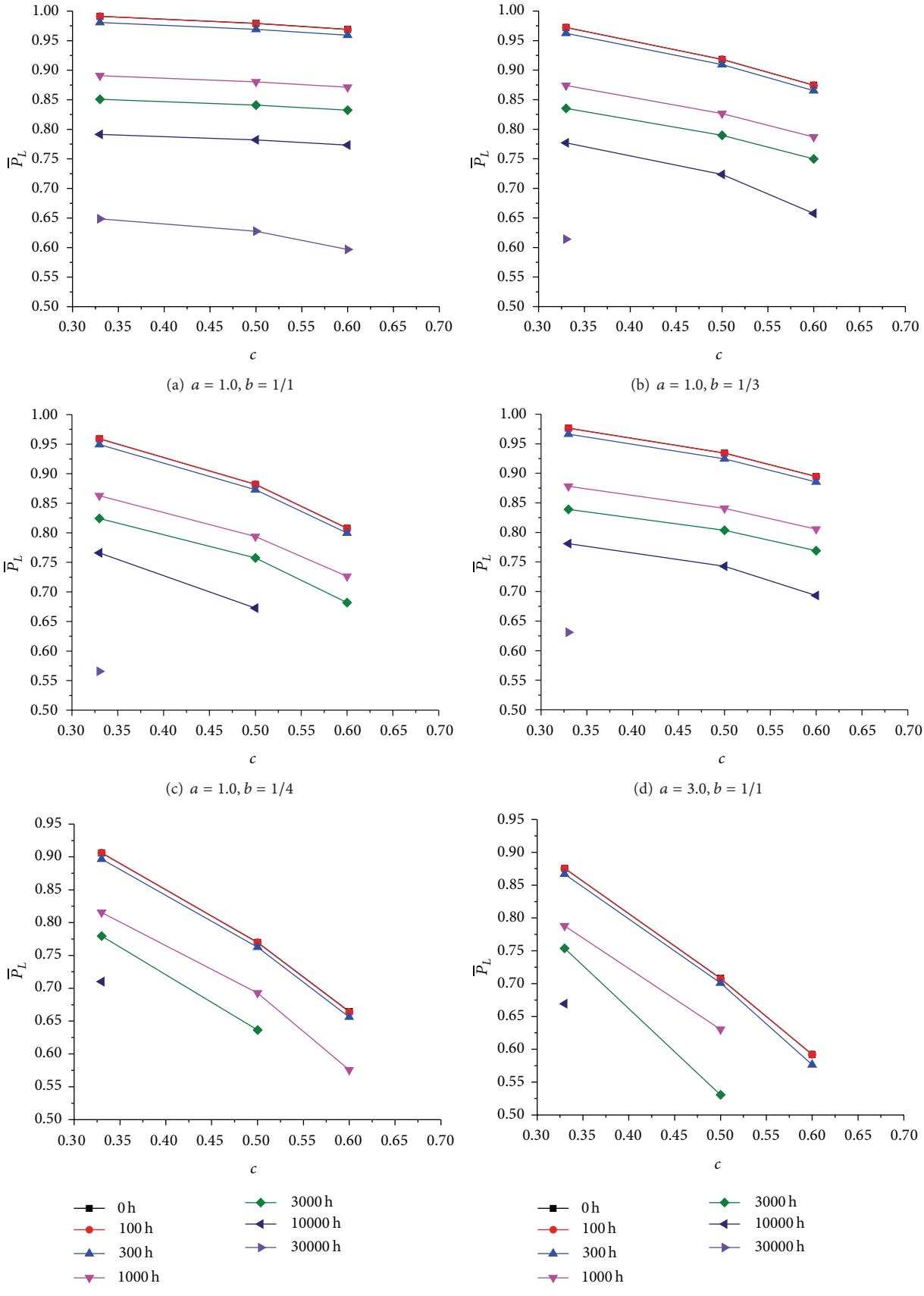


(a) $a = 1.0, b = 1/1$

(b) $a = 1.0, b = 1/3$

(c) $a = 1.0, b = 1/4$

(d) $a = 3.0, b = 1/1$

(e) $a = 3.0, b = 1/3$

(f) $a = 3.0, b = 1/4$

Figure 9: Continued.

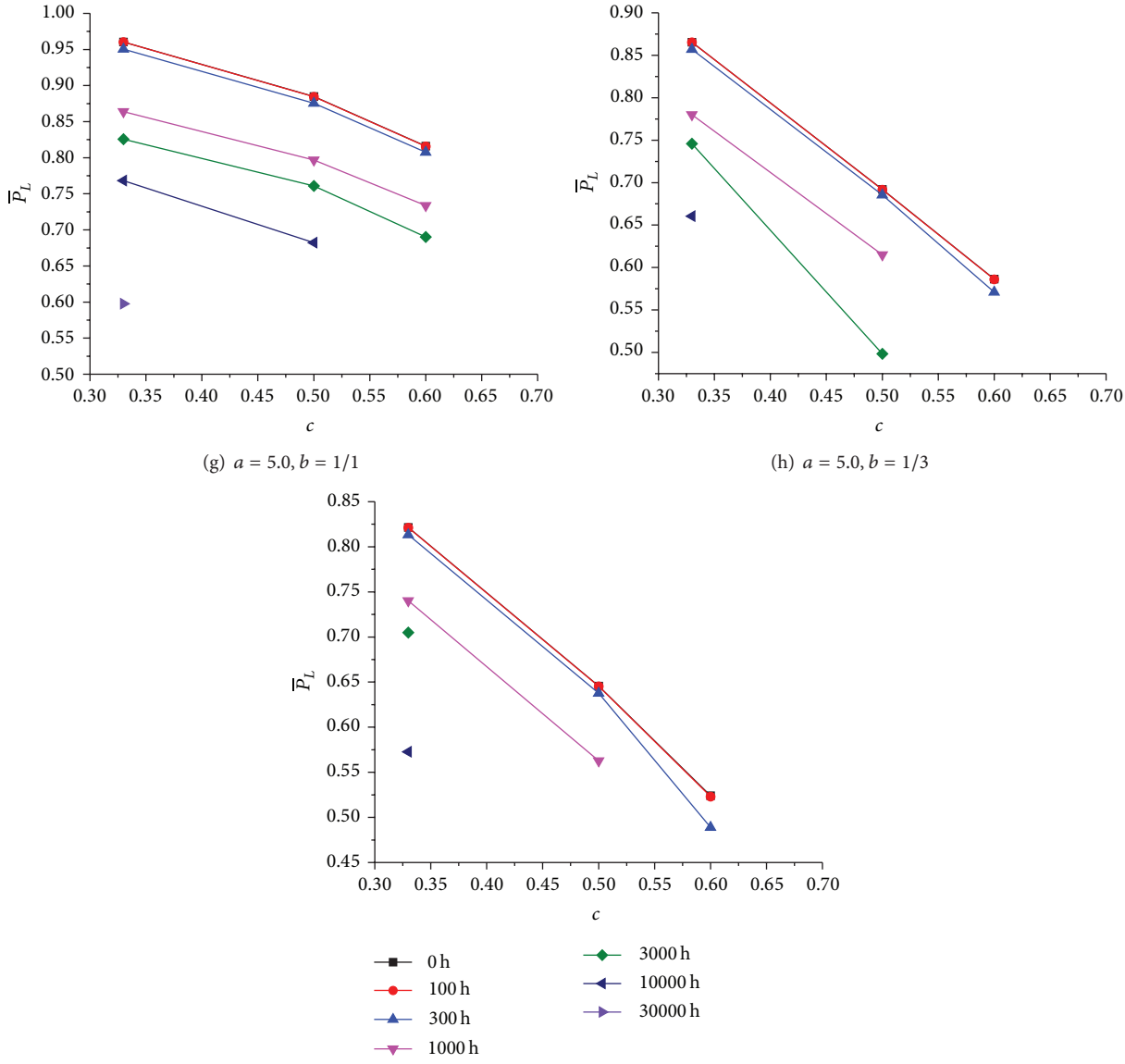


(g) $a = 5.0, b = 1/1$

(h) $a = 5.0, b = 1/3$

(i) $a = 5.0, b = 1/4$

Figure 9: Variations of limit load with volume defect dimensions.

defect, 27 shapes of defects and 190 computational examples were completed, and the results are listed in Table 5.

*3.2. Plastic Failure Modes.* The plastic failure mode of pressure vessel with volume defect under creep damage condition depends on the ratios $a$, $b$, and $c$ and dwell time $t$. When $K$ is constant, the extension of plastic zone of cylinder shell with volume defect parameter ratios which are $a = 1.0$, $b = 1/1$, and $c = 0.33$ when dwell time is between 0 and 30000 hours at 873 K is shown in Figures 5 and 6.

The results in Figures 4 and 5 show that the yield stress of 2.25Cr-1Mo steel at 873 K was reduced from 139 MPa to 100.86 MPa, and the maximum creep damage was increased from 0 to 0.217 when the dwell time was increased from 0 to 30000 hours. That indicated the yield stress had been reduced using USDFLD subroutine, the creep damage had been accumulated using CREEP subroutine, and the effective yield stress coupled time and creep damage had also been calculated and passed on ABAQUS successfully for limit load analysis using both of USDFLD and CREEP subroutines. The initial plastic zone was located in the bottom of spherical pit when the defect ratios were small ($a = 1.0$, $b = 1/1$, $c = 0.33$). With the internal pressure increasing, the plastic zone was expended along the axial direction until almost all the structure was yielding, which meant that the limit state was reached, and the failure mode of pressure vessel was overall structure plastic failure.

When $K$ is constant, the extension of plastic zone of cylinder shell with volume defect parameter ratios which are $a = 5.0$, $b = 1/4$, and $c = 0.33$ when dwell time is between 0 and 10000 hours at 873 K is shown in Figures 7 and 8.

The results in Figures 7 and 8 show that the yield stress of 2.25Cr-1Mo steel at 873 K was reduced from 139 MPa to 113.41 MPa, and the maximum creep damage was increased

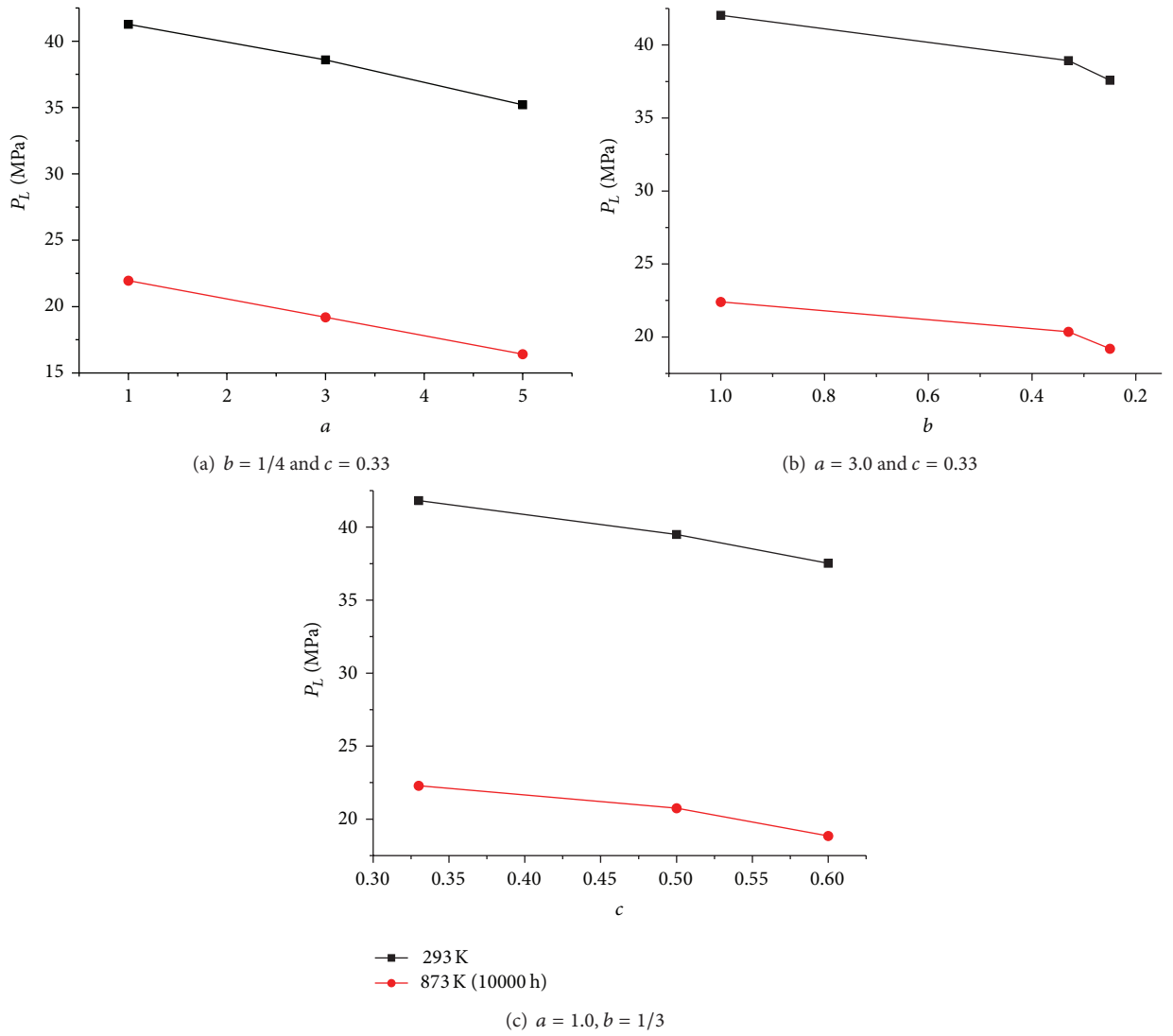


Figure 10: Comparisons of effect of the defect dimensions to the limit load between room temperature and high temperature.

from 0 to 0.358 when the dwell time was increased from 0 to 10000 hours. The plastic hinge was located in the ellipsoidal pit when the defect ratios are large ($a$ = 5.0, $b$ = 1/4, and $c$ = 0.33). With the internal pressure increasing, the locale plastic hinge was expended around the ellipsoidal pit. When the limit state was reached, the structure with this type of defect would leak in the plastic hinge zone, and the failure mode was local plastic failure.

It is important that dwell time was only up to 10000 hours, if the dwell time was larger than 12335 hours which is listed in Table 5, and the creep damage would exceed 1.0, which meant the structure was failure. At the same time, this phenomenon indicated that the service life of the pressure vessel structure at high temperature depends on the defect ratio seriously, which will be discussed in the next section.

*3.3. Parameter Analysis.* Figure 9 shows the effect of parameters of volume defect shapes to limit loads of cylindrical shell pressure vessel structure under high temperature.

It can be seen from Figure 9 that, with the increment of defect depth ratio $c$, the limit load decreased and the smaller the defect circumferential length ratio $b$ is, the faster the limit load decreased. In a similar way, the larger the defect axial length ratio $a$ is, the faster the limit load decreased. In other words, bigger volume defect would lead to higher creep damage accumulation and smaller limit load. It is also found that, limit load changed very slowly if the dwell time is less than 300 h, as yield stress of the material is not changed within 300 h and creep damage increased a little. From Figure 9(f) we can find that only one limit load is obtained at 10000 h when $a$ = 3.0, $b$ = 1/4, and $c$ = 0.33, if $c$ is larger than 0.33, and the limit load would be invalid because the structure is failed before 10000 h due to the creep damage.

Figure 10 shows the comparisons of effect of the defect dimensions to the limit load between room temperature and high temperature. Young's module $E$, Possion ratio $\nu$, and yield stress $\sigma_{s0}$ of 2.25Cr-1Mo steel at room temperature (293 K) are 210 GPa, 0.3, and 209 MPa, respectively [44].

Figure 10 shows the comparisons of effect of the defect dimensions to the limit load between room temperature and high temperature; it is found that limit load at room temperature is independent of service time as the creep damage is not considered. At the same time, effect of the defect dimensions to the limit load is almost the same between room temperature and high temperature.

## 4. Conclusions and Discussions

In this research, a numerical limit analysis of 2.25Cr-1Mo steel pressure vessel structure at 873 K has been studied. The creep behavior with K-R damage law has been implemented in ABAQUS with the CREEP and USDFLD subroutine. Meanwhile, 190 examples for the different sizes of volume defects of pressure vessels have been calculated, and the following conclusions can be drawn.

(1) The effective yield stress based on creep damage had been calculated and passed on ABAQUS successfully using both of USDFLD and CREEP subroutines, and numerical results indicate that the present approach for limit load analysis under high temperature was feasible.

(2) When the volume defect is small, the initial plastic zone is located in the bottom of spherical pit. With the internal pressure increasing, the plastic zone is expanded along the axial direction until almost all the structure is yielding, which means that the limit state is reached, and the failure mode of pressure vessel is overall structure plastic failure. When the volume defect is large, plastic hinge exists, which locates in the ellipsoidal pit. With the internal pressure increasing, the locale plastic hinge is expended around the ellipsoidal pit. When the limit state was reached, the structure with this type of defect would leak in the plastic hinge zone, and the failure mode was local plastic failure.

(3) The service life of the pressure vessel structure at high temperature depends on the defect ratio seriously, and bigger volume defect would lead to higher creep damage accumulation and smaller limit load. Limit load changed very slowly if the dwell time is less than 300 h, as yield stress of the material is not changed within 300 h and creep damage increased a little.

(4) In the present research, limit load under high temperature is defined as the load-carrying capacity after the structure serviced for a certain time. However, the limit load could be defined in another way, such as the maximum constant load during the whole service time with creep damage behavior at high temperature. This definition of limit load for pressure vessel at high temperature will be discussed and studied in the future work.

## Conflict of Interests

The authors declare that there is no conflict of interests regarding the publication of this paper.

## Acknowledgments

This work was supported by the National Science Foundation for Distinguished Young Scholars of China (Project no. 11325211) and the National Natural Science Foundation of China (Project no. 11302023).

## References

[1] M. Basirat, T. Shrestha, G. P. Potirniche, I. Charit, and K. Rink, "A study of the creep behavior of modified 9Cr–1Mo steel using continuum-damage modeling," *International Journal of Plasticity*, vol. 37, pp. 95–107, 2012.

[2] D. C. Drucker, "A more fundamental approach to plastic stress strain relations," in *Proceedings of the 1st U.S. National Congress of Applied Mechanics*, pp. 487–491, J.W. Edwards Publisher, Ann Arbor, Mich, USA, 1952.

[3] R. Hill, *The Mathematical Theory of Plasticity*, Oxford University Press, London, UK, 1950.

[4] P. G. Hodge, *Limit Analysis of Rotationally Symmetric Plates and Shells*, Prentice-Hall, Englewood Cliffs, NJ, USA, 1963.

[5] T. Belytschko and P. G. Hodge, "Plane stress limit analysis by finite elements," *Journal of the Engineering Mechanics Division*, vol. 96, no. 6, pp. 931–944, 1970.

[6] P. G. Hodge Jr., "Limit analysis with multiple load parameters," *International Journal of Solids and Structures*, vol. 6, no. 5, pp. 661–675, 1970.

[7] G. Maier and J. Munro, "Mathematical programming applications to engineering plastic analysis," *Applied Mechanics Reviews*, vol. 35, no. 12, pp. 1631–1643, 1982.

[8] D. C. A. Koopman and R. H. Lance, "On linear programming and plastic limit analysis," *Journal of the Mechanics and Physics of Solids*, vol. 13, no. 2, pp. 77–87, 1965.

[9] R. H. Lance and D. C. A. Koopman, *Limit Analysis of Shells of Revolution by Linear Programming*, Cornell University, Ithaca, NY, USA, 1967.

[10] G. Maier, A. Zavenlani-Rossi, and D. Benedetti, "A finite element approach to optimal design of plastic structures in plane stress," *International Journal for Numerical Methods in Engineering*, vol. 4, no. 4, pp. 455–473, 1972.

[11] E. Christiansen, "Computation of limit loads," *International Journal for Numerical Methods in Engineering*, vol. 17, no. 10, pp. 1547–1570, 1981.

[12] E. Christiansen and K. D. Andersen, "Computation of collapse states with von Mises type yield condition," *International Journal for Numerical Methods in Engineering*, vol. 46, no. 8, pp. 1185–1202, 1999.

[13] E. G. Berak and J. C. Gerdeen, "A finite element technique for limit analysis of structures," *Journal of Pressure Vessel Technology*, vol. 112, no. 2, pp. 138–144, 1989.

[14] G. Chen, *Numerical Limit and Shakedown Analysis of the Pressure Vessels with Part-Through Slots*, Tsinghua University, Beijing, China, 1994.

[15] D. Mackenzie, J. Shi, and J. T. Boyle, "Finite element modelling for limit analysis by the elastic compensation method," *Computers and Structures*, vol. 51, no. 4, pp. 403–410, 1994.

[16] Y. H. Liu, Z. Z. Cen, and B. Y. Xu, "A numerical method for plastic limit analysis of 3-D structures," *International Journal of Solids and Structures*, vol. 32, no. 12, pp. 1645–1658, 1995.

[17] Y. H. Liu, Z. Z. Cen, and B. Y. Xu, "Numerical limit analysis of cylindrical shells with part-through slots," *International Journal of Pressure Vessels and Piping*, vol. 64, no. 1, pp. 73–82, 1995.

[18] L. Yinghua, C. Zhangzhi, and X. Bingye, "Numerical investigation of the limit loads for pressure vessels with part-through slots," *Acta Mechanica Solida Sinica*, vol. 8, no. 3, pp. 263–276, 1995.

[19] S. Zhou, Y. Liu, and S. Chen, "Upper bound limit analysis of plates utilizing the C1 natural element method," *Computational Mechanics*, vol. 50, no. 5, pp. 543–561, 2012.

[20] S. Chen, Y. Liu, and Z. Cen, "Lower-bound limit analysis by using the EFG method and non-linear programming," *International Journal for Numerical Methods in Engineering*, vol. 74, no. 3, pp. 391–415, 2008.

[21] S. Chen, Y. Liu, and Z. Cen, "Lower bound shakedown analysis by using the element free Galerkin method and non-linear programming," *Computer Methods in Applied Mechanics and Engineering*, vol. 197, no. 45–48, pp. 3911–3921, 2008.

[22] L. Chen, Y. Liu, P. Yang, and Z. Cen, "Limit analysis of structures containing flaws based on a modified elastic compensation method," *European Journal of Mechanics A: Solids*, vol. 27, no. 2, pp. 195–209, 2008.

[23] Y. H. Liu, X. F. Zhang, and Z. Z. Cen, "Lower bound shakedown analysis by the symmetric Galerkin boundary element method," *International Journal of Plasticity*, vol. 21, no. 1, pp. 21–42, 2005.

[24] P. Yang, Y. Liu, Y. Ohtake, H. Yuan, and Z. Cen, "Limit analysis based on a modified elastic compensation method for nozzle-to-cylinder junctions," *International Journal of Pressure Vessels and Piping*, vol. 82, no. 10, pp. 770–776, 2005.

[25] Y. Liu, X. Zhang, and Z. Cen, "Numerical determination of limit loads for three-dimensional structures using boundary element method," *European Journal of Mechanics A: Solids*, vol. 23, no. 1, pp. 127–138, 2004.

[26] B. F. Dyson and M. S. Loveday, "Creep fracture in nimonic 80A under triaxial tensile stressing," in *Creep in Structures*, A. R. S. Ponter and D. R. Hayhurst, Eds., pp. 406–421, Springer, Berlin, Germany, 1981.

[27] K. D. Al-Faddagh, G. A. Webster, and B. F. Dyson, "Influence of state of stress on creep failure of 2.25%Cr–1%Mo steel," in *Mechanical Behaviour of Materials IV*, pp. 289–295, 1984.

[28] D. Wu, E. M. Christian, and E. G. Ellison, "Influence of constraint on creep stress distribution in notched bars," *Journal of Strain Analysis for Engineering Design*, vol. 19, no. 4, pp. 209–220, 1984.

[29] A. K. Ray, K. Diwakar, B. N. Prasad, Y. N. Tiwari, R. N. Ghosh, and J. D. Whittenberger, "Long term creep-rupture behaviour of 813 K exposed 2.25-1Mo steel between 773 and 873 K," *Materials Science and Engineering A*, vol. 454-455, pp. 124–131, 2007.

[30] S. Goyal, K. Laha, C. R. Das, S. Panneerselvi, and M. D. Mathew, "Finite element analysis of effect of triaxial state of stress on creep cavitation and rupture behaviour of 2.25Cr-1Mo steel," *International Journal of Mechanical Sciences*, vol. 75, pp. 233–243, 2013.

[31] M. Yatomi, K. M. Nikbin, and N. P. O'Dowd, "Creep crack growth prediction using a damage based approach," *International Journal of Pressure Vessels and Piping*, vol. 80, no. 7-8, pp. 573–583, 2003.

[32] M. Yatomi, N. P. O'Dowd, K. M. Nikbin, and G. A. Webster, "Theoretical and numerical modelling of creep crack growth in a carbon-manganese steel," *Engineering Fracture Mechanics*, vol. 73, no. 9, pp. 1158–1175, 2006.

[33] M. Yatomi, C. M. Davies, and K. M. Nikbin, "Creep crack growth simulations in 316H stainless steel," *Engineering Fracture Mechanics*, vol. 75, no. 18, pp. 5140–5150, 2008.

[34] M. Yatomi and M. Tabuchi, "Issues relating to numerical modelling of creep crack growth," *Engineering Fracture Mechanics*, vol. 77, no. 15, pp. 3043–3052, 2010.

[35] C. S. Oh, N. H. Kim, S. H. Min, and Y. J. Kim, "Finite element damage analysis for predictions of creep crack growth," in *Proceedings of the ASME Pressure Vessels and Piping Division/K-PVP Conference*, Washington, DC, USA, 2010.

[36] C.-S. Oh, N.-H. Kim, Y.-J. Kim, C. Davies, K. Nikbin, and D. Dean, "Creep failure simulations of 316H at 550°C: part I—a method and validation," *Engineering Fracture Mechanics*, vol. 78, no. 17, pp. 2966–2977, 2011.

[37] M. McLean and B. F. Dyson, "Modeling the effects of damage and microstructural evolution on the creep behavior of engineering alloys," *Journal of Engineering Materials and Technology, Transactions of the ASME*, vol. 122, no. 3, pp. 273–278, 2000.

[38] L. M. Kachanov, "Rupture time under creep conditions," *International Journal of Fracture*, vol. 97, no. 1–4, pp. 11–18, 1999.

[39] Y. N. Rabotnov, *Creep Problems in Structural Members*, North-Holland, Amsterdam, The Netherlands, 1969.

[40] D. R. Hayhurst, P. R. Dimmer, and C. J. Morrison, "Development of continuum damage in the creep rupture of notched bars," *Philosophical Transactions of the Royal Society of London A*, vol. 311, no. 1516, pp. 103–129, 1984.

[41] ABAQUS Version 6.13, Dassault Systèmes, Providence, RI, USA, 2013.

[42] T. H. Hyde, A. A. Becker, and W. Sun, "Validation of finite element approaches for modelling creep continuum damage mechanics," in *Proceedings of the 7th International Conference on Computational Structures Technology*, B. H. V. Topping and C. A. Mota Soares, Eds., paper 62, Civil-Comp Press, Stirlingshire, UK, 2004.

[43] ASME, *ASME Boiler & Pressure Vessel Code Division 1-Subsection NH III*, ASME, 2010.

[44] ASME, *ASME Boiler & Pressure Vessel Code II Part D Properties (Customary) Materials*, ASME, 2010.